J. Acoust. Soc. Am., **40**, 86 (1966).
13. Nierode, D. E., Ph.D. thesis, Univ. Wisconsin, Madison (1968).
14. Romer, I. C., Jr., *J. Acous. Soc. Am.*, **34**, 192 (1966).
15. Hilsenrath, J., "Tables of Thermodynamic and Transport Properties of Air, Argon, Hydrogen, Nitrogen, Oxygen and Steam," Permagon Press, New York (1960).
16. "JANAF Thermochemical Tables," (PB--168-370) Springfield, Va. Clearing House (1965).
17. "International Critical Tables," McGraw-Hill, New York (1930).
18. "Handbook of Chemistry and Physics," Chemical Rubber Publishing Co., Cleveland, Ohio (1959).
19. Wilke, C. R., *J. Chem. Phys.*, **18**, 517 (1950).
20. El-Hakeem, A. S., Ph.D. thesis, Univ. Wisconsin, Madison (1965).
21. Douslin, D. R., *Prog. Int. Res. Thermo. Trans. Prop., ASME*, 135 (1962).
22. Nelson, L. C., and E. F. Obert, *AIChE J.*, **1**, 74 (1955).

Manuscript received October 8, 1968; revision received November 18, 1968; paper accepted November 20, 1968.

A Statistical Model of a Porous Medium with Nonuniform Pores

R. E. HARING
Esso Production Research Company

and R. A. GREENKORN
Purdue University, Lafayette, Indiana

A random network model of a porous medium with nonuniform pores has been constructed. Nonuniformity is achieved by assigning two-parameter distributions to pore radius and pore length. Statistical derivations result in expressions for bulk model properties which are consistent with known empirical behavior of porous media such as capillary pressure, hydraulic permeability, and longitudinal and transverse dispersion. A series of experiments is suggested whereby the parameters of porous media structure may be determined from observed macroscopic behavior by using the expressions developed in this paper.

This study describes a simple model of the structure of a porous medium with nonuniform pores. There are models, statistical in nature, which describe the microstructure of porous catalysts (*4, 6, 9, 15, 18, 21*). (Darcy's law may not be valid for flow in the microstructures.) These models are generally capillary unit cell models. The appropriate mass transfer equation is integrated to find effectiveness factors for these porous catalysts. The model described herein is for bulk phenomena associated with a pressure gradient (Darcy's law is valid) rather than diffusion due to a concentration gradient. Previous statistical models for describing bulk phenomena did not include nonuniformity (*5, 10, 17*). Real porous media even though seemingly homogeneous* and isotropic are most often nonuniform, and this nonuniformity may affect the observable bulk phenomena. A parametric statistical model is used to calculate macroscopic properties of the medium such as capillary pressure, permeability, and dispersion in order to relate these properties to the structure of the model. A pore can be described in terms of its radius, length, and orientation in a flow field. The model is constructed of two-parameter distribution functions. The parameters of these distribution functions may be related to the physical properties of the prototype structure. Orientation is random with all directions allowed. Various properties of a porous medium are found by integrating over the joint distributions resulting from the model so constructed. Random walk of particles of fluid is used to describe macroscopic dispersion during laminar flow through the model. Finally, the results are discussed in view of experimental data and continuum theories to examine the effect of nonuniformity on the observable phenomena. These studies, more experimental data, and extensions to heterogeneous anisotropic models are necessary to understand and develop a more general theory of dispersion in real porous media.

THE MODEL

The model pore space is approximated by a large number of randomly oriented, straight, cylindrical pores. The elemental pore in this network is presented in Figure 1 as a straight cylinder of length l and radius r. The pore is oriented in space by an angle θ from the z axis (the direction of flow) and by an angle ψ which is the angle between the y axis and the projection of the center line of the pore in the x-y plane. We assume for this study that all directions of an elemental pore are equally likely and $0 \leq \theta \leq \frac{\pi}{2}$, $0 \leq \psi \leq 2\pi$. The model can be constructed in terms of dimensionless quantities by defining

$$l^* = \frac{l}{L}; \quad 0 \leq l \leq L \quad \text{and} \quad 0 \leq l^* \leq 1 \tag{1}$$

and

$$r^* = \frac{r}{R}; \quad 0 \leq r \leq R \quad \text{and} \quad 0 \leq r^* \leq 1 \tag{2}$$

Both L and R must be finite in a real porous medium.

To make the model nonuniform, the dimensionless length l^* and dimensionless radius r^* are each assumed to be distributed according to the beta function (*11*).

$$f(x; p_1, p_2) = \frac{(p_1 + p_2 + 1)!}{p_1!\, p_2!} (x)^{p_1} (1 - x)^{p_2} \tag{3}$$

where p_1 and p_2 are arbitrary parameters. The beta function was selected as the probability distribution function for both radius and length, since the random variables have a range of zero to one and the distribution has a spectrum of skew and symmetric shapes depending on the choice of the parameters. Familiar two-parameter distributions (for example, normal, chi squared, etc.) lack flexibility to simulate natural petrographic phenomena and particularly suffer from the shortcomings of infinite range which are contrary to Equations (1) and (2).

If we assume the radius, length, and orientation of the elemental pores to be independent,† then the probability

* In a flow sense homogeneous means no distortion of bulk streamlines from flow in a homogeneous potential field.

† In a uniform, isotropic medium of constant porosity, length and radius are dependent (through pore volume). In general, radius and length are not dependent.

Table 1. Calculated Values of Dispersion (square centimeters per second) for Various Values of the Parameters of the Beta Distribution (Velocity = 0.1 cm./sec.)

a	b	α	β	$K_L \times 10^3$	$K_T \times 10^4$	K_L/K_T
2	2	0	0	1.77	4.85	3.66
2	2	−½	−½	7.28	7.87	9.37
2	2	−½	1	33.2	16.8	19.8
2	2	2	4	4.82	6.54	7.40
2	2	2	2	3.78	5.87	6.42
2	2	4	2	2.43	4.89	4.96
2	2	1	1	4.54	6.32	7.18
2	4	2	4	3.96	5.15	7.70
4	2	2	4	4.30	5.98	7.20
2	4	1	1	4.78	4.96	9.65
4	2	1	1	7.95	11.6	6.85
2	4	4	2	2.02	4.00	5.05
4	2	4	2	4.26	8.95	4.76
1	1	4	2	1.98	4.28	4.68
1	1	2	4	3.54	5.75	6.16

distribution function for length and radius are

$$f(l^*) = \frac{(a+b+1)!}{a!b!}(l^*)^a(1-l^*)^b \tag{4}$$

and

$$g(r^*) = \frac{(\alpha+\beta+1)!}{\alpha!\beta!}(r^*)^\alpha(1-r^*)^\beta \tag{5}$$

The average values for l^* and r^* are found from the first moment of the distribution function to be

$$<l^*> = \frac{a+1}{a+b+2} = \frac{<l>}{L} \tag{6}$$

and

$$<r^*> = \frac{\alpha+1}{\alpha+\beta+2} = \frac{<r>}{R} \tag{7}$$

The model is conceived as a large number of randomly intersecting elemental pores. The probability a given pore exists with size in the range $l^* \to l^* + dl^*$, $r^* \to r^* + dr^*$, $\theta \to \theta + d\theta$, and $\psi \to \psi + d\psi$ is given by the normalized product of the independent probabilities such that

$$dE = \underbrace{\frac{1}{2\pi}}_{\text{normalization}} \underbrace{\frac{(a+b+1)!}{a!b!}(l^*)(1-l^*)^b\,dl^*}_{\substack{\text{probability} \\ l^* \to l^* + dl^*}} \underbrace{\frac{(\alpha+\beta+1)!}{\alpha!\beta!}(r^*)^\alpha(1-r^*)^\beta\,dr^*}_{\substack{\text{probability} \\ r^* \to r^* + dr^*}} \underbrace{\sin\theta\,d\theta\,d\psi}_{\substack{\text{probability} \\ \theta \to \theta + d\theta \\ \psi \to \psi + d\psi}} \tag{8}$$

PROPERTIES OF THE MODEL

Capillary Pressure

The capillary pressure in a partially saturated pore is

$$P_c = \frac{2\sigma\cos\omega}{r} \tag{9}$$

Since the capillary pressure of a pore depends on its radius, the capillary pressure of an ensemble of pores will depend on the distribution of pore radii in the ensemble. The differential volume of fluid invading the pore space of the model increased by a fractional saturation dS is $V_p\,dS$. This saturation change results from fluids entering all pores in the model of radius r^* and

$$V_p dS = -\underbrace{N}_{\substack{\text{No. of} \\ \text{pores}}} \underbrace{\pi R^2 L r^{*2} <l^*>}_{\substack{\text{vol. of pores} \\ \text{of radius r}^*}}, \underbrace{g(r^*)\,dr^*}_{\substack{\text{probability of a} \\ \text{pore of radius } r^*}} \tag{10}$$

Equation (10) is equivalent to

$$dS = -\frac{R^2 L}{V_p} N\pi r^{*2} <l^*> g(r^*)\,dr^* \tag{10a}$$

or

$$dS = -\frac{N\pi r^{*2} <l^*> g(r^*)\,dr^*}{N\pi <r^{*2}> <l^*>} \tag{10b}$$

and

$$dS = -\frac{r^{*2}}{<r^{*2}>} g(r^*)\,dr^* \tag{10c}$$

Since r^* and l^* are assumed independent, we can use the average length of the ensemble of pores. As the radius of a pore becomes smaller, according to Equation (9), the capillary pressure associated with it and its saturation will increase. Therefore, as the radius varies from 0 to 1, saturation varies from 1 to 0. Integrating Equation (10) after substituting Equation (5) for the radius and the second moment of the distribution function

$$<r^{*2}> = \frac{(\alpha+1)(\alpha+2)}{(\alpha+\beta+2)(\alpha+\beta+3)} \tag{10d}$$

we get

$$1 - S = \int_0^{r^*} \frac{(\alpha+\beta+3)!}{(\alpha+2)!\beta!}(r^*)^{\alpha+2}(1-r^*)^\beta\,dr^* \tag{11}$$

The invading fluid does not have access to all pores when $r^* \to 1$. The error involved diminishes rapidly as S increases (5). We ignore this error.

Combine the definition of r^*, Equation (2), and the capillary pressure, Equation (9), to give

$$r^* = \frac{r}{R} = \frac{P_c(R)}{P_c(r)} = \frac{1}{P_c^*} \tag{12}$$

which normalizes P_c with respect to the threshold pressure corresponding to the largest pore. Substitute Equation (12) into Equation (11):

$$1 - S = \int_0^{\frac{1}{P_c^*}} \frac{(\alpha+\beta+3)!}{(\alpha+2)!\beta!}\left(\frac{1}{P_c^*}\right)^{\alpha+2}\left(1-\frac{1}{P_c^*}\right)^\beta d\left(\frac{1}{P_c^*}\right) \tag{13}$$

The values for the incomplete beta function

$$B(x; p_1, p_2) = \int_0^x \frac{(p_1+p_2+1)!}{p_1!p_2!}x^{p_1}(1-x)^{p_2}\,dx \tag{14}$$

are tabulated (13) so a curve of P_c^* vs. $(1 - S)$ may be constructed by using the tabulated values for

$$(1-S) = B\left(\frac{1}{P_c^*};\ \alpha+2, \beta\right) \tag{15}$$

Figure 2 shows radius distribution functions for a uniform and a wide pore radius distribution. The capillary pressure curves determined from Equation (15) for these two distributions are in Figure 3. The results of Figure 3 agree qualitatively with published data on capillary pressures (16) and exactly with results from network models (5). We measured the drainage capillary pressure of a 590- to 840-μ glass bead pack (porosity 35.4%). The parameters for the radius distribution function were determined from the threshold pressure corresponding to the largest pore, that is, at $(1 - S) = 1$. Figure 4 compares the experimental data with the results calculated

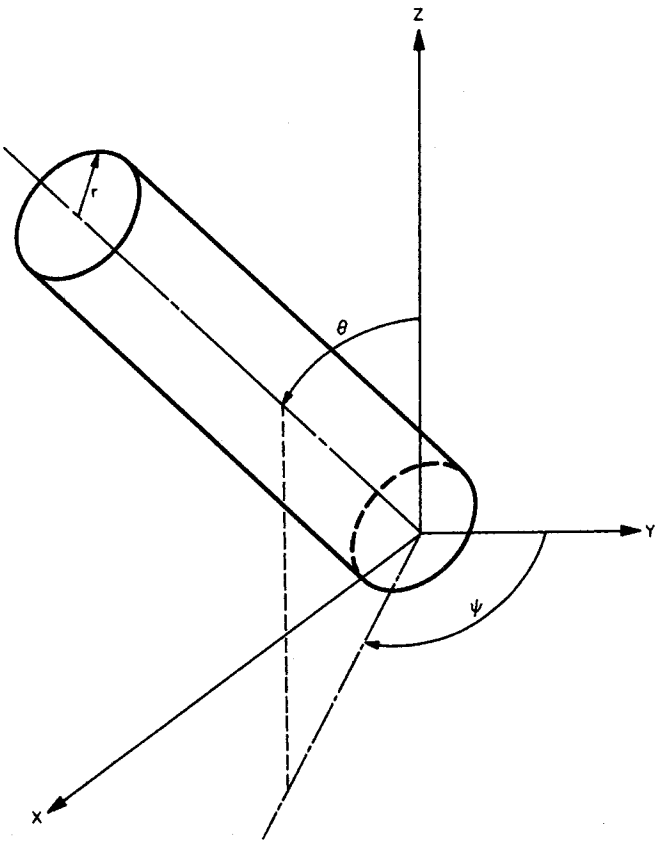

Fig. 1. Description of the elemental pore space.

from Equation (15). The experimental and calculated results agree to 90% (where the slope of the curve approaches infinity).

Permeability

The permeability of the model is found by relating the average velocity in an elemental pore to the average velocity in the ensemble. Consider bulk flow through the model only in the z direction; then, according to the Hagen-Poiseuille equation

$$v = -\frac{R^2}{8\mu} r^{*2} \frac{\partial p}{\partial z} \cos\theta \tag{16}$$

The components of this velocity are

$$\left.\begin{aligned} v_x &= v \sin\theta \sin\psi \\ v_y &= v \sin\theta \cos\psi \\ v_z &= v \cos\theta \end{aligned}\right\} \tag{17}$$

The average velocities in each direction for the ensemble of pores is found by integrating the velocity components of Equation (17) over the entire range of pore sizes and orientations such that

$$\left.\begin{aligned} \langle v_x\rangle &= \int_E v \sin\theta \sin\psi \, dE \\ \langle v_y\rangle &= \int_E v \sin\theta \cos\psi \, dE \\ \langle v_z\rangle &= \int_E v \cos\theta \, dE \end{aligned}\right\} \tag{18}$$

where dE is given by Equation (8) and the integration limits are the range of l^*, r^* θ, and ψ. The integration for the average velocities in the x and y direction is

$$\left.\begin{aligned} \langle v_x\rangle &= 0 \\ \langle v_y\rangle &= 0 \end{aligned}\right\} \tag{19}$$

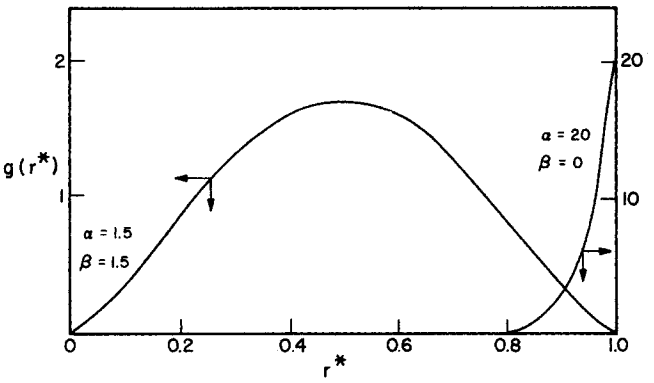

Fig. 2. Radius distribution function.

The average velocity in the z direction is

$$\langle v_z\rangle = -\frac{R^2}{24\mu} \frac{\partial p}{\partial z} \frac{(\alpha+2)(\alpha+1)}{(\alpha+\beta+3)(\alpha+\beta+2)} \tag{20}$$

The average pore velocity for a fluid flowing in porous medium is given by Darcy's law and the Dupuit-Forchheimer equation (*19*):

$$V = -\frac{k}{\phi\mu} \frac{\partial p}{\partial z} \tag{21}$$

Since $\langle v_z\rangle \equiv V$, Equations (20) and (21) are combined, and

$$\frac{k}{\phi} = \frac{R^2}{24} \frac{(\alpha+2)(\alpha+1)}{(\alpha+\beta+3)(\alpha+\beta+2)} \tag{22}$$

or, in terms of average radius

$$\frac{k}{\phi} = \frac{\langle r\rangle^2}{24} \frac{(\alpha+2)(\alpha+\beta+2)}{(\alpha+\beta+3)(\alpha+1)} \tag{23}$$

The permeability estimated for the glass beads used for the capillary pressure of Figure 4 estimated from Equation (23), with values of α and β estimated from the threshold pressure, is 160 darcies. The measured permeability value for the bead pack is 175 darcies.

Dispersion

A cloud of marked particles flowing through a porous medium will disperse owing to convection. This convective dispersion is a result of the tortuous and circuitous nature of the flow paths in a porous medium. For most flow situations of interest to engineers, the residence time of the fluid in an individual pore is much smaller than the time necessary for appreciable mixing due to molecular diffusion within that pore. If we assume the residence time is small enough such that the effect of molecular diffusion is negligible, expressions for the dispersion coefficients of the model can be found by determining the probability distribution of the position of a marked particle after a random walk of independent steps through the model (*2*). The problem is reduced to one of deciding which pore a marked particle will select when it arrives at a junction of two or more pores. At each junction the probability of path choice must be related to the probability of existence of a pore dE, Equation (8), and to the velocity distribution at the junction. The possibilities we considered are that the choice is proportional to the velocity v given by Equation (16) and the volumetric rate q integrated from Equation (16). For each possibility we have the further possibilities; the average microscopic streamline is selected and the streamline is selected proportional to the velocity distribution $K\left[1-\left(\frac{\hat{r}}{r}\right)^2\right]$.

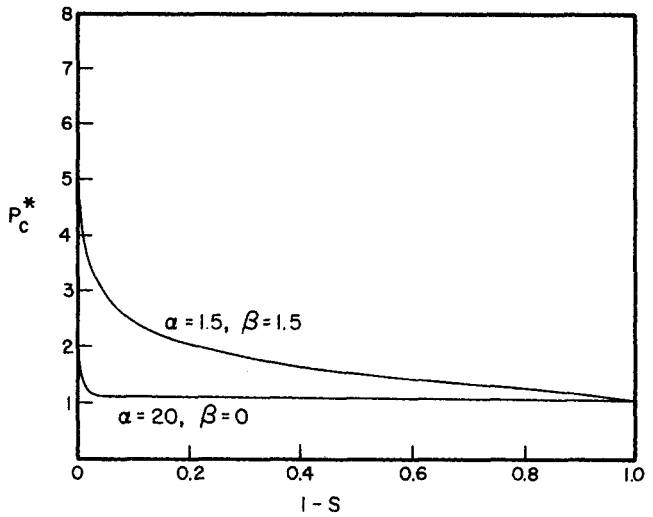

Fig. 3. Capillary pressure curves from Figure 2 distributions.

Since we cannot identify streamlines with this model, and, furthermore, we cannot assume a particle will jump streamlines on shifting pores (laminar flow is assumed), it is reasonable to select the average streamline. The choice between the differential (v) and integral (q) form of the Hagen-Poiseuille law appears to be arbitrary. Physically it is more realistic to use q. The results calculated for the choice of v (7) differ from the choice used here (q) by a two integer shift of the parameter α.† Therefore, the probability of path choice is assumed as

$$dP = \frac{q}{M}\,dE = \frac{v\pi r^2}{M}\,dE \tag{24}$$

Substituting (2), (8). and (16) into (24) and normalizing since the integral over dP must equal unity, we get

$$dP = \frac{\sin\theta\cos\theta}{\pi}\,\frac{(a+b+1)!}{a!b!}\,(l^*)^a(1-l^*)^b$$
$$\frac{(\alpha+\beta+5)!}{(\alpha+4)!\beta!}\,(r^*)^{\alpha+4}(1-r^*)^\beta\,d\psi\,d\theta\,dl^*\,dr^* \tag{25}$$

The longitudinal and transverse dispersion coefficients are defined in terms of the variance of the longitudinal and transverse displacements and the time required for such displacements, such that for the model discussed here

$$K_L = \frac{\overline{(Z-\tilde{V}T)^2}}{2T} \tag{26}$$

and

$$K_T = \frac{\overline{X^2}}{2T} = \frac{\overline{Y^2}}{2T} \tag{27}$$

where $\overline{(Z-\tilde{V}T)^2}$, $\overline{X^2}$, $\overline{Y^2}$ are the variances of the average displacements in the z, x, and y directions. (Since we are discussing flow in the z direction, $\overline{X^2} = \overline{Y^2}$). We can find the statistical displacement functions after a large number of steps n (see Appendix),†† but, according to

† We preempt and mention that with the choice of v the expressions for dispersion include the terms α, $\alpha - 1$ in the denominator which require limiting α to values other than 0 and 1. For a choice of q this limitation is not necessary. On the other hand, the choice of v gives the result that a particle following the most probable path is transported with the average velocity.

†† Equation numbers with prefix A are derived in the Appendix which has been deposited as document 00868 with the ASIS National Auxiliary Publications Service, c/o CCM Information Sciences, Inc., 22 W. 34th St., New York 10001 and may be obtained for $1.00 for microfiche or $3.00 for photocopies. The term J is defined in the Appendix. $J = \frac{(\alpha+1)(\alpha+2)(\alpha+\beta+4)(\alpha+\beta+5)}{(\alpha+3)(\alpha+4)(\alpha+\beta+2)(\alpha+\beta+3)}$

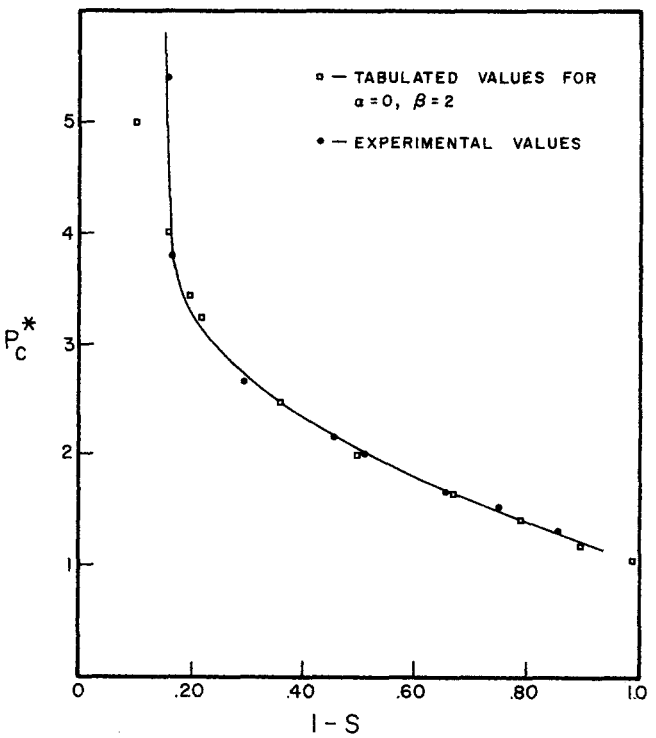

Fig. 4. Comparison of measured and calculated capillary pressure.

Equations (26) and (27), we need the statistical properties after a fixed time. It has been shown that the probability distribution function for the dimensionless time for time fixed and the number of steps variable coincides with the probability distribution function for the dimensionless time with the time variable and the number of steps fixed when n is very large (17).

Define Y as the displacement in the y direction after a time T corresponding to a large n of order $\bar{n}$; then, from Equations (A-15), (A-16), and (A-30)†

$$\overline{Y^2} = LVT\left[\frac{3}{8}\,\frac{(a+2)}{(a+b+3)J}\right] \tag{28}$$

and the transverse dispersion coefficient from Equation (27) is

$$K_T = \frac{3}{16}\,\frac{(a+2)(a+b+2)}{(a+1)(a+b+3)J}\cdot\langle l\rangle V \tag{29}$$

The same value of K_T results by using $\overline{X^2}$.

Define Z as the displacement in the z direction after a time T corresponding to large n of order $\bar{n}$. Substitute Equations (A-29)† and (A-30)† into Equation (A-19) to give

$$Z = \frac{VT}{J} - \tau\left[\frac{3}{2}\,\frac{(a+b+2)}{(a+1)J^3}\,LVT\right]^{1/2} + \rho\left[\frac{3}{2}\,\frac{(a+b+2)}{(a+1)J}\,LVT\right]^{1/2} \tag{30}$$

Further, considering (A-10)† and the consequences of (A-19)† through (A-22)†, we get

$$\overline{(Z-\tilde{V}T)^2} = \frac{3}{2}\,\frac{(a+b+2)}{(a+1)J}\,LVT\left[\frac{\sigma_T^2}{J^2} + \sigma_Z^2 - 2\,\frac{\sigma_{ZT}^2}{J}\right] \tag{31}$$

The longitudinal dispersion coefficient from Equations (26), (A-28)†, (A-13)†, and (A-23)† is, therefore

° See footnote on column 1.

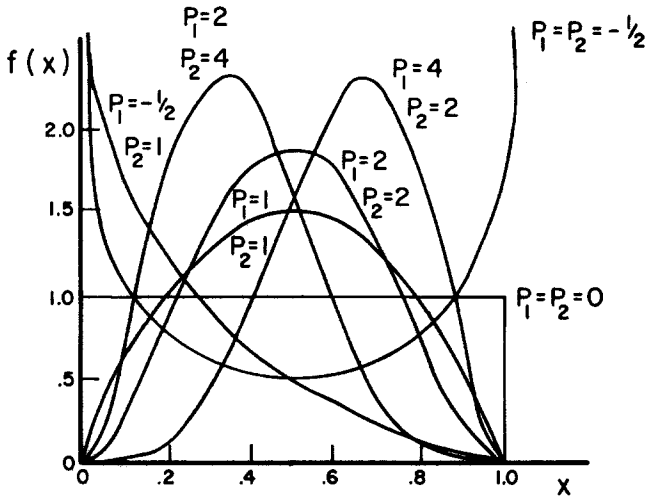

Fig. 5. Beta distribution.

$$K_L = \frac{1}{12}\frac{(a+2)(a+b+2)}{(a+1)(a+b+3)J^2}\langle l\rangle V \ln \left[\frac{27}{2}\frac{(a+b+2)^2}{(a+1)^2J^3}\frac{VT}{\langle l\rangle}\right] \quad (32)$$

The expressions for K_L and K_T, Equations (32) and (29), reduce to the results for uniform length and radius if $a, \alpha >> 1$ and $b, \beta = 0$. The values of K_L and K_T for nonuniform pores are larger than predicted on the basis of average pore length $\langle l\rangle$. The longitudinal dispersion coefficient K_L is more sensitive to nonuniform pore properties than the transverse coefficient. Both coefficients depend on the parameters of pore length and radius distribution, as well as on average pore length. When probability of path choice is taken proportional to velocity (7) instead of flux as used here, the transverse dispersion coefficient is independent of pore radius distribution. The ratio K_L/K_T is virtually independent of pore length distribution but is a function of pore radius distribution:

$$\frac{K_L}{K_T} = \frac{4}{9J}\ln\left[\frac{27}{2}\frac{(a+b+2)^2}{(a+1)^2J^3}\frac{VT}{\langle l\rangle}\right] \quad (33)$$

The argument of the logarithm in Equations (32) and (33) is proportional to the average number of pores (or path changes) of the prototype porous medium.

Figure 5 shows the beta distribution for several sets of values of the parameters p_1 and p_2. The values for K_L, K_T, and K_L/K_T calculated from Equations (29) and (32) and (33) for the various distribution function in Figure 5 are given in Table 1. These values correspond qualitatively to measured values in porous media of various degrees of nonuniformity. For a uniform, unconsolidated, isotropic media, one would expect a value of K_L/K_T approaching 3 (*12*). For consolidated media, the pore radius distribution will be severely skewed which leads to higher values of K_L/K_T.

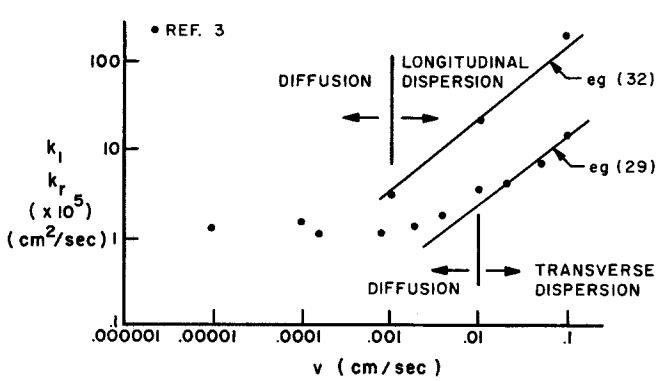

Fig. 6. Comparison of measured and calculated dispersion for glass beads.

In general, for unconsolidated porous media, depending on skewness of the distribution function, we would expect K_L/K_T to be from 3 to 10, and for consolidated media we would expect much higher values (3, *13*).

We matched values of the longitudinal and transverse dispersion for unconsolidated 0.025-cm. glass beads (average) using Equations (29) and (32) and data reported in the literature (*3*). We assumed a symmetrical length distribution where $a = 2$, $b = 2$ with an average length of 0.0062 cm. which assumes the largest pore is one-half the bead diameter.* The radius distribution was assumed skewed with $\alpha = 2$ and $\beta = 4$. This radius distribution is similar to the one used to fit the capillary pressure data of Figure 4. The calculated results are compared to the experimental values in Figure 6. The calculated ratio of K_L/K_T is 10.9.

We matched the longitudinal and transverse dispersion for a consolidated berea sandstone by assuming a length distribution of $a = 2$, $b = 4$ and a radius distribution of $\alpha = -\frac{1}{2}$, $\beta = 6$. For consolidated media, the length distribution is moderately skewed, and the pore sized distribution resembles a gamma function. The two distributions selected have these characteristics. The average length was assumed as 0.00188 cm. The calculated results are compared with the experimental values in Figure 7. The calculated ratio of K_L/K_T is 61.5.†

Equation (33) predicts that the ratio of longitudinal to transverse dispersion is independent of velocity but proportional to the length of the media. Although literature data (*3, 8*) indicate a slight velocity dependence on the ratio of K_L/K_T, it is not clear that the transverse dispersion coefficients reported are completely independent of diffusion (that is, velocity is not high enough).

DISCUSSION

Data on capillary pressure (*16*) and dispersion coefficients (*3, 14*) of porous media with both uniform and nonuniform pores qualitatively support the properties of the model derived in this paper. Figures 4, 6, and 7 quantitatively support the model. The shapes of capillary drainage curves for real media with monomodal pore distributions are remarkably similar to shapes generated by Equation (13). Empirical relations for both longitudinal and transverse dispersion coefficients in laminar flow, where molecular diffusion is negligible, show that these coefficients are proportional to bulk velocity, porous media particle diameter, and a heterogeneity factor. This is essentially what is shown by Equations (29) and (32). The argument of the logarithm in Equation (32) is proportional to length of the porous media. This logarithmic dependency has not been verified in the published literature, perhaps because of lack of data over a sufficiently large length range for the same media. The two-parameter distributions for pore length and radius result in explicit expressions for the heterogeneity factor. The aver-

* We assume the smaller beads fall between the larger ones; thus the largest pore will not be maximum bead diameter.

† To calculate the dispersion, we selected the distribution parameter which seemed to describe the media. We could adjust the parameter to get a better fit in Figures 6 and 7. To use the model in a way that does not allow adjusting parameters, we need a complete suite of measurements which are described in the next section. We can, of course, curve fit data and use the model to infer the structure of the media.

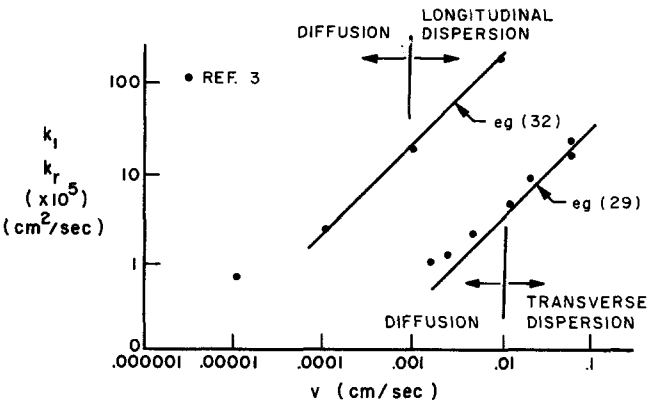

Fig. 7. Comparison of measured and calculated dispersion for berea sandstone.

age pore length appearing in this model is not necessarily equal to media particle diameter but is a sufficient length parameter with perhaps more physical significance.

The foregoing discussion leads to an interesting possibility for a series of experiments to determine the parameters of the statistical model presented herein. Perform capillary pressure, permeability, and porosity measurements on a homogeneous porous media. Also, measure transverse and longitudinal dispersion coefficients in laminar flow at several velocities where molecular diffusion is negligible. Further, repeat the longitudinal dispersion measurements in media samples of several different lengths. The shape of the capillary pressure curve will be a function of α and β from Equation (13). If the ratio K_L/K_T is plotted vs. the logarithm of media length, the slope will also be a function of α and β from Equation (33). Thus α and β can be obtained. Permeability and porosity measurements are used with Equation (23) to determine $<r>$, the average pore radius. The extrapolation of K_T/K_L to unity media length results in a function of a, b, and $<l>$, the average pore length, since α and β have been established, as is seen from Equation (33). Substitution of this function of a, b, and $<l>$ in Equations (29) and (32) as well as previously determined values for α and β will lead to yet another function of a, b, and $<l>$. This function is determined from the proportionality between K_T and V and K_L and V at a given media length. If reasonable estimates of $<l>$ can be made from photographic inspection of media thin sections and Equation (6), the complete suite of parameters are determined from phenomenological behavior. To the authors' knowledge, no such complete set of data exists.

Bear (*1*) has shown that for the mean flow in an arbitrary direction, the variance of dispersion D_{ij} and the displacement L_{kl} are related by the transformation

$$D_{ij} = a_{ijkl} L_{kl} \tag{34}$$

where the summation convention for Cartesian tensors applies, and a_{ijkl} is the geometric dispersivity tensor. For a homogeneous isotropic porous medium, the a_{ijkl} reduces to an expression which depends on only two constants, a_I and a_{II}. The usual equation for concentration change during flow in a porous medium is

$$\frac{\partial c}{\partial t} = \frac{\partial}{\partial x_i} D_{ij} \frac{\partial c}{\partial x_j} - V_i \frac{\partial c}{\partial x_i} \tag{35}$$

or, in terms of the value a_I and a_{II} (*20*), the expression for a homogeneous isotropic porous medium is

$$\frac{\partial c}{\partial t} = a_I V \frac{\partial^2 c}{\partial x_1^2} + a_{II} V \frac{\partial^2 c}{\partial x_2^2} + a_{II} V \frac{\partial^2 c}{\partial x_3^2} \tag{36}$$

and, therefore

$$a_I V = D_I$$
$$a_{II} V = D_{II} \tag{37}$$

where D_I and D_{II} are the longitudinal and transverse coefficients of dispersion (the principal values of D_{ij}). Equation (37) is valid for flow in one direction, and D_I and D_{II} are equivalent to the K_L and K_T of Equations (32) and (29).

To fully investigate the theory of dispersion, the dependence of the longitudinal dispersion coefficient on the size of n must be investigated. Other models might be found for evaluating the variance of T_n to alter the form. The effects of heterogeneity, that is, the use of several distributions simultaneously for the pore radius and length distributions, should be studied. Anisotropy could be included in the model by limiting the range of the orientation angles.

CONCLUSIONS

A statistical model of a porous medium with nonuniform pores has been constructed which matches experimental capillary pressure, permeability, and dispersion data. Several interesting properties are predicted from such a model. As one might expect, saturation is a function of capillary pressure and the parameters of flow radius distribution. The permeability-porosity ratio is a function of the average radius squared and the pore radius distribution. Thus, the permeability-porosity ratio causes dissipation due to entrance-exit effects. The dispersion coefficient is dependent on the parameters of both the pore radius and length distribution. Therefore, one would expect dispersion to change as a function of nonuniformity of the medium, even though the average resistance and tortuosity are constant. Furthermore, given a pore length distribution, the tortuosity is constant. Finally, for a nonuniform medium, a particle following the most probable path is transported through the medium at a velocity different from the Darcy velocity by a factor which is a function of the flow radius distribution.

ACKNOWLEDGMENT

R. A. Greenkorn was partially supported during the early part of this study by a grant from the Petroleum Research Fund. Acknowledgment is made to the donors of the Petroleum Research Fund, administered by the American Chemical Society, for partial support of this research. The latter part of this study was supported under research grant VIP 01048-01 from the Federal Water Pollution Control Administration, United States Department of the Interior.

We also wish to thank the Esso Production Research Company for their interest and support.

NOTATION

a, b = parameters in length distribution
a_{ijkl} = dispersivity tensor
c = concentration
D_{ij} = dispersion tensor
k = permeability
K_L = longitudinal dispersion
K_T = transverse dispersion
l = pore length
L = length of longest pore
L_{kl} = displacement tensor
M = normalization constant
n = number of steps
p = pressure
P_c = capillary pressure

q = volumetric flow rate
r = pore radius
R = radius of largest pore
$\hat{r}$ = particular radius within pore
S = saturation
T = time
v = velocity
V = average pore velocity
V_p = pore volume
$\tilde{V}$ = velocity along most probable path
X,Y,Z = displacements in the x, y, z directions

Greek Letters

α, β = parameters in radius distribution
ϕ = porosity
ψ = angle from y axis projected in xy plane
ρ,ζ,η = dimensionless coordinates
θ = angle from z axis
σ = surface tension
σ^2 = variance
τ = dimensionless time
μ = viscosity
ω = angle of wetting

Subscripts

T = time
Z = coordinate, z direction

LITERATURE CITED

1. Bear, J., *J. Geophys. Res.*, **66**, 1185 (1961).
2. Chandrasekhar, S., *Rev. Mod. Phys.*, **15**, 1 (1943).
3. Grane, F. E., and G. N. F. Gardner, *J. Chem. Eng. Data*, **6**, 283 (1961).
4. Evans, R. B., G. M. Watson, and E. A. Mason, *J. Chem. Phys.*, **35**, 2076 (1961).
5. Fatt, I., *Petrol. Trans. Am. Inst. Mining Engrs.*, **207**, 144 (1956).
6. Foster, R. N., and J. B. Butt, *AIChE J.*, **12**, 180 (1966).
7. Haring, R. E., M.S. thesis, Univ. Tulsa, Okla. (1961).
8. Harleman, D. R. J., and R. R. Rumer, *J. Fluid Mech.*, **16**, 385 (1963).
9. Hoogschagan, J., *Ind. Eng. Chem.*, **47**, 906 (1955).
10. Josselin de Jong, G., *Trans. Am. Geophys. Union*, **39**, 67 (1958).
11. Mood, A., "Introduction to the Theory of Statistics," McGraw-Hill, New York (1950).
12. Patel, R. D., and R. A. Greenkorn, *AIChE J.*, to be published.
13. Pearson, K., ed., "Tables of the Incomplete Beta-Function," The University Press, Cambridge, England (1934).
14. Perkins, T. K., Jr., and O. C. Johnston, *Petrol. Trans. Am. Inst. Mining Engrs.*, **228**, 70 (1963).
15. Petersen, E. E., *AIChE J.*, **4**, 343 (1958).
16. Purcell, W. R., *Petrol. Trans. Am. Inst. Mining Engrs.*, **186**, 39 (1949).
17. Saffman, P. G., *J. Fluid Mech.*, **7**, 194 (1960).
18. Satterfield, C. N., and T. K. Sherwood, "The Role of Diffusion in Catalysis," Addison-Wesley, Reading, Mass. (1963).
19. Scheidegger, A. E., "The Physics of Flow Through Porous Media," Macmillan, New York (1957).
20. Scheidegger, A. E., *J. Geophys. Res.*, **66**, 3273.
21. Wakao, N., and J. M. Smith, *Chem. Eng. Sci.*, **17**, 825 (1962).

Manuscript received May 10, 1968; revision received October 9, 1968; paper accepted November 4, 1968.

Birefringent Flow Visualization of Transitional Flow Phenomena in an Isosceles Triangular Duct

RICHARD W. HANKS and JAMES C. BROOKS

Brigham Young University, Provo, Utah

A flow visualization study was made with an optically birefringent solution of milling yellow dye in water flowing through a transparent duct of isoceles triangular cross section. The present data confirm a number of theoretical predictions concerning transitional phenomena in triangular ducts. One of the most interesting of these phenomena is the existence of a region of simultaneous laminar and turbulent flow in the duct. The present results, which agree with the theory, indicate an order of laminar and turbulent flow which is inverse to previous observations made with smoke filament tracings.

The phenomena associated with the transition from laminar to turbulent motion have been a subject of increasing interest to researchers in fluid mechanics since Reynolds (*1*) first performed his classical dye injection studies. The dye injection technique of Reynolds has since proved a tempting means of making visible the properties of flowing streams and for visualization of the properties of turbulent eddies in transitional flow (*2* to *9*). Although the method seems simple, it is not without its pitfalls.

This technique was used (*4*, *5*) in a series of studies performed with pipes and concentric annuli in which dye filaments were injected into a flowing water stream from a series of bent needle injectors.* As a result of these

J. C. Brooks is with the Fluor Corporation, Los Angeles, California.

* These injectors resembled a Pitot tube turned downstream. They consisted of hypodermic needle tubing having a 90° bend near their terminus with the bent portion extending downstream parallel to the duct boundary. Dye was forced through these tubes and into the flowing stream.